Rapid Communications

Hydrogen as a source of flux noise in SQUIDs

Zhe Wang,[1] Hui Wang,[2,*] Clare C. Yu,[2,*] and R. Q. Wu[1,2,*]

[1]*State Key Laboratory of Surface Physics, Key Laboratory of Computational Physical Sciences, and Department of Physics, Fudan University, Shanghai 200433, China*

[2]*Department of Physics and Astronomy, University of California, Irvine, California 92697, USA*

(Received 21 September 2017; published 9 July 2018)

Superconducting qubits are hampered by flux noise produced by surface spins from a variety of microscopic sources. Recent experiments indicated that hydrogen (H) atoms may be one of those sources. Using density functional theory calculations, we report that H atoms either embedded in, or adsorbed on, an α-$Al_2O_3(0001)$ surface have sizable spin moments ranging from 0.81 to 0.87μ_B with energy barriers for spin reorientation as low as $\sim$10 mK. Furthermore, H adatoms on the surface attract gas molecules such as O_2, producing new spin sources. We propose coating the surface with graphene to eliminate H-induced surface spins and to protect the surface from other adsorbates.

DOI: 10.1103/PhysRevB.98.020403

Superconducting circuits have a wide variety of applications, e.g., photon detectors used in astrophysics [1], bolometers involved in dark matter searches [2], nanomechanical motion sensors [3], cavity quantum electrodynamics [4,5], and quantum limited parametric amplifiers [6]. However, their performance continues to be impaired by noise and dielectric loss produced by microscopic defects. While progress has been made [7–9], identifying microscopic sources of noise remains a top priority. Of particular interest as a qubit is the superconducting quantum interference device (SQUID) [10] where a major problem is low-frequency $1/f$ flux noise generated by fluctuating spins residing on the surface of normal metals [11], superconductors [12,13], and insulators [14]. Proposed microscopic sources of spins have included surface spin clusters and correlated fluctuations [15,16], electron spin exchange via the hyperfine interactions [17], and adsorbed OH or O_2 molecules [18,19]. In particular, the suggestion of adsorbed O_2 molecules [19] has been supported by experimental measurements involving x-ray magnetic circular dichroism (XMCD) as well as measurements of susceptibility and flux noise [7]. Efforts to remove adsorbed O_2 molecules have significantly reduced the flux noise in SQUIDs, but have not completely eliminated it, implying that there are additional sources of flux noise [7]. Recent experiments have implicated hydrogen (H) atoms as a source of flux noise [8,20] even though hydrogen is rarely associated with magnetism. Electron spin resonance (ESR) measurements find an energy splitting of $\sim$1.42 GHz on sapphire [α-$Al_2O_3(0001)$], a common substrate often used as a model of the native oxide layer on Al SQUIDs. 1.42 GHz coincides with the hyperfine splitting of a free H atom. To explain this observation and to find ways to eliminate magnetic noise in Al SQUIDs, we investigated the magnetic states of different arrangements of H atoms inside aluminum oxides and on their surface.

In this work, we used density functional theory (DFT) to investigate H atoms as a source of flux noise on α-$Al_2O_3(0001)$. H atoms can occupy interstitial sites in bulk sapphire or be adsorbed on various surface sites. In either case they can produce a sizable local magnetic moment. H atoms on α-$Al_2O_3(0001)$ facilitate the adsorption of other molecules such as O_2 that can produce additional fluctuating spins. The binding energies of H adatoms and $H + O_2^-$ coadsorbates are large and hence cannot be easily removed through heating. We propose that the flux noise from H atoms can be reduced by coating the α-$Al_2O_3(0001)$ surface with graphene to remove unpaired electrons from H/α-$Al_2O_3(0001)$ and prevent other magnetic species from being adsorbed.

Our DFT calculations used the projector augmented wave method implemented in the Vienna *ab initio* Simulation Package (VASP) [21,22]. Exchange-correlation interactions were included using the generalized-gradient approximation with the Perdew-Burke-Ernzerhof (PBE) functional [23]. The α-$Al_2O_3(0001)$ surface was modeled with a slab consisting of 18 atomic Al and O layers and a vacuum gap 15 Å thick. A $3 \times 3 \times 1$ Monkhorst-Pack mesh [24] was used to sample the Brillouin zone to optimize the 2×2 supercell with the criterion that the force acting on each atom was less than 0.01 eV/Å. The van der Waals correction was implemented using the PBE-optB86b functional [25]. The energy cutoff for the plane-wave expansion was set to 600 eV, as in our previous studies of H [26,27]. For direct comparison with experiment, the x-ray absorption spectroscopy (XAS) and XMCD spectra, as well as the ESR frequencies were calculated using the full potential linearized augmented plane-wave) method [28,29]. To identify plausible sources of $1/f$ noise, we calculated the magnetic anisotropy energy (MAE), which is the energy barrier for spin rotation. To determine the MAE at the microelectron volt (μeV) level, we used torque methods [30] that evaluate the expectation values of angular derivatives of the Hamiltonian with respect to the polar angle θ and azimuthal angle ϕ of the spin moment, i.e., $\tau(\theta) = \frac{\partial E_{\text{total}}(\theta)}{\partial \theta} = \sum_{\text{occ}} \langle \psi_{i,\boldsymbol{k}} | \frac{\partial H_{\text{SO}}}{\partial \theta} | \psi_{i,\boldsymbol{k}} \rangle$, as in studies of magnetic molecules and magnetostrictive alloys [31,32].

*Corresponding authors: huiw2@uci.edu; cyu@uci.edu; wur@uci.edu

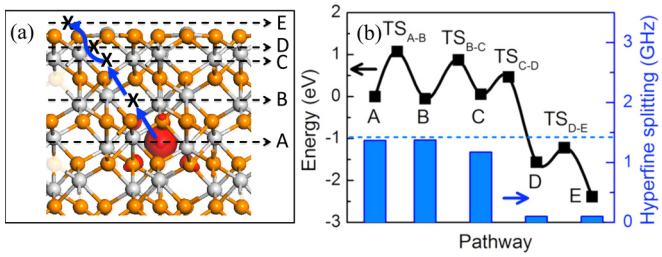

FIG. 1. (a) Left panel shows the spin density of an H atom embedded in α-Al_2O_3(0001). The gray and orange balls represent Al and O atoms, respectively. The spin density of the embedded H atom is represented by red isosurfaces ($0.05e/Å^3$). Black crosses show the positions along the diffusion path (blue arrows) for the embedded H atom heading toward the surface, with A, B, C, D, and E denoting the interstitial sites in different layers. (b) Left axis shows the relative total energy of an H atom diffusing from interior sites to the surface. Energies at $TS_{A\text{-}B}$, $TS_{B\text{-}C}$, $TS_{C\text{-}D}$, and $TS_{D\text{-}E}$ indicate the diffusion barriers between two adjacent interstitial sites. Right axis shows the calculated ESR values corresponding to each interstitial site. The horizontal blue dashed line represents the experimental ESR value [8].

Adsorbed hydrogen comes from atmospheric H_2 or H_2O molecules. So we examined the adsorption and dissociation of H_2 and H_2O molecules on α-Al_2O_3(0001) and found that H_2 binds weakly (binding energy ~ -0.14 eV) while H_2O binds strongly (binding energy ~ -1.15 eV) to the α-Al_2O_3(0001) surface. *Ab initio* molecular dynamics (AIMD) simulations demonstrate that H_2 can be easily desorbed from the surface, whereas H_2O tends to disassociate into OH and H (see Figs. S1 and S2 in the Supplemental Material [33]), consistent with previous reports [34]. Al samples and their thin native oxide layers likely contain a small amount of atomic H under ambient conditions [35–37]. As depicted in Fig. 1(a), atomic H can be easily trapped in cagelike interstitial sites in α-Al_2O_3. According to our climbing image-nudged elastic band simulations [38], the energy barrier for an H atom diffusing from the interior along the path indicated in Fig. 1(a) is as high as $\sim$1.07 eV [Fig. 1(b)]. Our AIMD simulations at 300 K demonstrate that H atoms do not escape from a cage deep inside bulk sapphire on a timescale of 4 ps [see Fig. S3(a) [33]]. Thus, H atoms (denoted H_{inters}) in Al SQUIDs can occupy interstitial sites in the oxide layer and be adsorbed on the surface. (Note that H is nonmagnetic in metallic Al.) So we will focus on the energetic and magnetic properties of interstitial H atoms embedded in different layers of bulk α-Al_2O_3 as well as adsorbates on the surface.

H_{inters} interacts weakly with adjacent atoms, thus retaining its atomic properties. Figure 1(a) shows the large spin density around H_{inters} with a moment $\sim 0.87\mu_B$. Our calculations with large unit cells show that there are antiferromagnetic interactions between H_{inters} atoms in α-Al_2O_3(0001), with exchange energies of -0.12 meV($\sim$1.4 K) when the separation between two H_{inters} is 4.8 Å, and -0.03 meV ($\sim$0.4 K) for a separation of 9.6 Å (see Table I). The MAE of H_{inters} is smaller than 1 μeV ($<$10 mK), which is almost beyond the limit of DFT approaches, indicating that the spin orientation energy is virtually isotropic. According to our previous Monte Carlo simulations of classical anisotropic XY spins [19], this implies that H_{inters} atoms can produce $1/f$ flux noise.

The native oxide layer on Al is typically very thin and H_{inters} atoms are likely to be driven to the surface by the large energy difference between the bulk and the surface [see Fig. 1(b)]. Energy barriers gradually decrease as H_{inters} approaches the surface of α-Al_2O_3(0001). AIMD simulations of H_{inters} atoms embedded in interstitial sites near the surface [layer C in Fig. 1(a)] demonstrated that they drift to the oxygen site on the α-Al_2O_3(0001) surface within 5 ps at 600 K, which is consistent with experiment [8] [see Fig. S3(b) [33]]. Therefore, the apparent density of H_{inters} should be low under ambient conditions. However, an experiment on a thick sapphire sample by de Graaf *et al.* [8] found a strong ESR signal at $\sim$1.42 GHz, indicating a rather high density of atomic H ($\sim 2.2\times10^{17}$ m^{-2}). Our calculations found that the ESR hyperfine splitting for H_{inters} atoms embedded in different layers of sapphire is between 1.28 and $\sim$1.36 GHz [see Fig. 1(b)], very close to the experimental measurement of de Graaf *et al.* [8]. A peak in the flux noise of an Al/sapphire fluxmon qubit at $\sim$1.4 GHz was also reported by Quintana *et al.* [20], which may be due to spin fluctuations of interstitial H atoms. Therefore, the flux noise from H_{inters} atoms could be reduced by annealing at high temperatures [8].

Since both the outward segregation of H_{inters} and the dissociation of H_2O may result in H atoms on the α-Al_2O_3(0001) surface, we found the preferred adsorption sites and binding energies of an H adatom using

$$E_b = E_{H/Al_2O_3(0001)} - E_{Al_2O_3(0001)} - E_H. \quad (1)$$

$E_{H/Al_2O_3\ (0001)}$ and $E_{Al_2O_3\ (0001)}$ are the total energies of the α-Al_2O_3(0001) slab with and without an H atom, respectively. E_H is the total energy of the free H atom. By considering an H atom adsorbed on top of O, Al, and O-O bridge sites,

TABLE I. Calculated exchange interaction energies, commonly denoted by J, at different separations for H_{inters}, $H_{atop\text{-}O}$, $H_{atop\text{-}Al}$, $H_{atop\text{-}O} + O_2^-$, and O_2 molecules in or on α-Al_2O_3(0001). The data for O_2 molecules comes from previous studies [19]. Positive values correspond to ferromagnetic interactions and negative values to antiferromagnetic interactions.

	4.8 Å	9.6 Å
H_{inters} (this work)	-0.12 meV (1.4 K)	-0.03 meV (0.4 K)
$H_{atop\text{-}O}$ (this work)	-5.05 meV (60.6 K)	-0.01 meV (0.1 K)
$H_{atop\text{-}Al}$ (this work)	0.73 meV (8.8 K)	0.02 meV (0.2 K)
$H_{atop\text{-}O} + O_2^-$ (this work)	-0.17 meV (2.0 K)	-0.1 μeV($\sim$0 K)
O_2 molecule	0.14 meV (1.7 K)	0.05 meV (0.6 K)

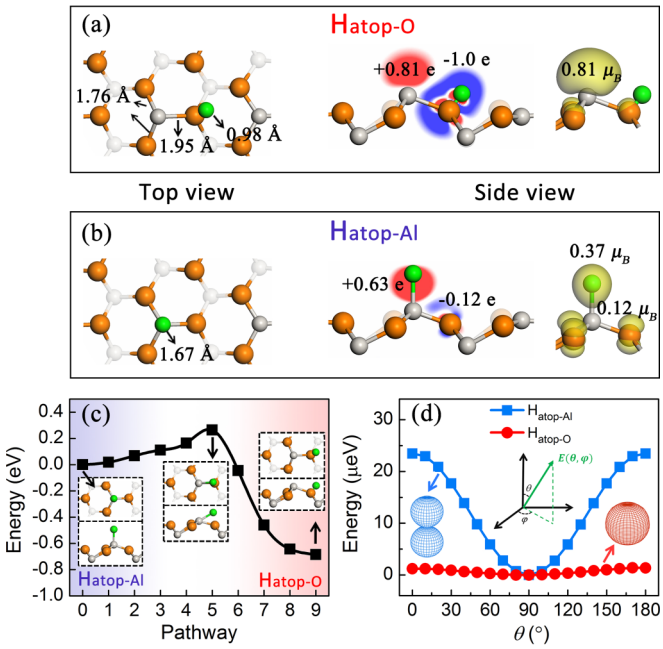

FIG. 2. (a) Schematic geometries of an H atom adsorbed on the O site of an α-Al_2O_3(0001) surface. Only atoms near the adsorption site are shown. The gray, orange, and green balls depict Al, O, and H atoms. Charge depletion and accumulation are represented by blue and red, respectively. The lime-green isosurface depicts the distribution of spin density. (b) The same as (a) but with an H atom adsorbed on the Al site of an α-Al_2O_3(0001) surface. (c) Reaction pathway of the H adatom hopping from the $H_{atop\text{-}Al}$ site to the $H_{atop\text{-}O}$ site. The horizontal dashed lines indicate the energy barrier. Insets show the top and side views of atomic arrangements corresponding to different states. (d). Relative total energy versus the polar angle θ of the spin direction with respect to the surface normal for the $H_{atop\text{-}O}$ (red line) and $H_{atop\text{-}Al}$ geometries (blue line) on an α-Al_2O_3(0001) surface. The left and right insets show the isoenergy surfaces of the MAE versus the polar and azimuthal angles that are sketched in the central inset.

we found that the most stable site is on top of the oxygen atom on the α-Al_2O_3(0001) surface (denoted as "$H_{atop\text{-}O}$") [see Fig. 2(a)]. The binding energy and bond length of H-O are about -1.07 eV and 0.98 Å, respectively. Another stable but less desirable adsorption site for H is on top of the surface Al site (denoted as "$H_{atop\text{-}Al}$") [see Fig. 2(b)] with an H-Al bond length of 1.67 Å and a binding energy of -0.39 eV. The energy barrier is $\sim$0.26 eV for the conversion from $H_{atop\text{-}Al}$ to $H_{atop\text{-}O}$ and is 0.94 eV in the reverse process [see Fig. 2(c)]. From these numbers the $H_{atop\text{-}Al}$ geometry occurs much less frequently than $H_{atop\text{-}O}$ for H adatoms on the α-Al_2O_3(0001) surface.

Our Bader charge analysis indicates that the $H_{atop\text{-}O}$ adatom donates its charge to the adjacent O atoms (0.16e) and to the neighboring Al atom (0.81e), as depicted by the charge redistribution in Fig. 2(a). As a result, the topmost Al atom is strongly magnetized with a spin moment of $\sim 0.81\mu_B$, with a spin density distribution shown in Fig. 2(a). In contrast, $H_{atop\text{-}Al}$ gains electrons from the Al atom underneath it and the three neighboring O atoms [see the charge redistribution in Fig. 2(b)]. This results in magnetic moments of $0.37\mu_B$ and $0.12\mu_B$ for the H atom and each of the three surface O atoms, respectively. As shown in Fig. 2(d), the MAE is almost isotropic for $H_{atop\text{-}O}$, implying easy spin fluctuations in every direction. For $H_{atop\text{-}Al}$, the calculated MAE between the spin orientation in and out of the surface plane is about $-24\,\mu$eV, showing that the easy axis lies in the surface plane. The energy barrier to spin rotation in the surface plane is extremely small [$\sim 1\,\mu$eV or 10 mK].

The noise spectrum depends on spin-spin interactions. As shown in Table I, our DFT calculations with 2×2 and 4×4 supercells indicate $H_{atop\text{-}O}$ atoms interact antiferromagnetically on α-Al_2O_3(0001), with exchange energies of -5.05 meV ($\sim$60.6 K) when the separation between two $H_{atop\text{-}O}$ atoms is 4.8 Å, and -0.01 meV ($\sim$0.1 K) for a separation of 9.6 Å. In contrast, the $H_{atop\text{-}Al}$-induced magnetic moments interact ferromagnetically, with exchange energies of 0.73 meV ($\sim$8.8 K) when two $H_{atop\text{-}Al}$ atoms have a separation of 4.8 Å, and 0.02 meV ($\sim$0.2 K) for a separation of 9.6 Å. Together with the small MAE discussed above, both $H_{atop\text{-}O}$ and $H_{atop\text{-}Al}$ could produce $1/f$ magnetic flux noise.

Which H configuration dominates the flux noise on α-Al_2O_3(0001)? From the energetics in Figs. 1 and 2 for H segregation and adsorption, we find that the order of apparent densities (n) of H atoms in or on α-Al_2O_3(0001) is $n(H_{atop\text{-}O}) > n(H_{inters}) > n(H_{atop\text{-}Al})$. Our ESR calculations of the hyperfine splitting for $H_{atop\text{-}O}$ is essentially zero, due to the complete depletion of its charge. The hyperfine splitting for $H_{atop\text{-}Al}$ is 0.53 GHz, but this was not seen experimentally, consistent with our estimate of its small concentration. The surface to volume ratio implies that the ESR measurements [8] are dominated by the much more numerous H atoms embedded in the thick sapphire bulk, rather than by the surface spins.

Although $H_{atop\text{-}O}$ by itself is not magnetic, we found that $H_{atop\text{-}O}$ adatoms can attract other molecules from the atmosphere to the surface. In previous studies, we identified O_2 molecules as a possible source of $1/f$ noise [19], but these can either be removed by raising the temperature above 50 K due to the small binding energy (~ -0.15 eV per molecule) or avoided by protecting the surface with molecules that have a higher binding energy such as ammonia [7,19]. In the presence of $H_{atop\text{-}O}$, the binding energy of an O_2 molecule next to an H adatom increases to around -2.9 eV, mainly due to significant charge rearrangement. In the most stable geometry, the O_2 bond lies almost parallel to the α-Al_2O_3(0001) surface as shown in Fig. 3(a), and gains a charge of 1.0e from the surrounding Al atoms to become "O_2^-". The O-O bond length stretches by 16%, which is very different from the adsorption of an O_2 molecule on a bare α-Al_2O_3(0001) surface. The calculated magnetic moment of the $H_{atop\text{-}O} + O_2^-$ complex is $1.0\mu_B$, with an easy axis along the O-O bond and an MAE of $\sim 26\,\mu$eV ($\sim$0.30 K). This magnetic complex is a possible noise source and should form easily if $H_{atop\text{-}O}$ is present.

Note that de Graaf *et al.* suggested O_2^- as the possible source of the central peak in their ESR experiment [8], but there are a number of possibilities since $g = 2.0$ is characteristic of many spin systems. One way to experimentally confirm our prediction of $H_{atop\text{-}O} + O_2^-$ on α-Al_2O_3(0001) would be with XAS and XMCD spectra. According to our DFT calculations, the energies of the two π^*_{2p} states of O_2 are split into two as an additional electron is transferred from an Al atom to the

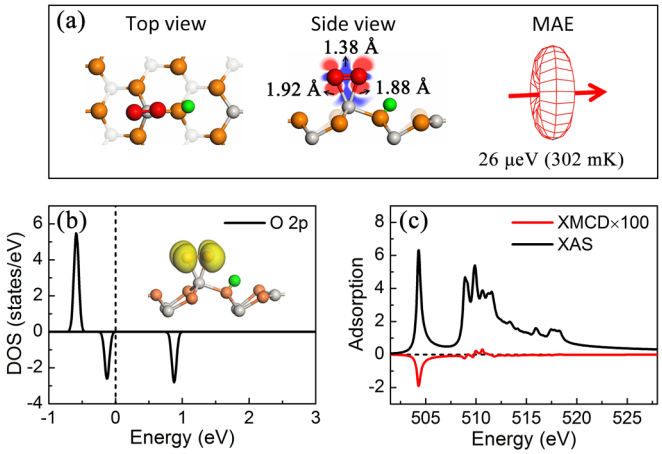

FIG. 3. (a) The atomic geometry and charge redistribution of an O_2^- molecule adsorbed on $H_{atop\text{-}O}/\alpha$-$Al_2O_3(0001)$. Al, O, and H atoms are colored as in Fig. 1. $E_{tot}(\theta,\varphi)$ is given in the right figure, with an arrow indicating the easy axis. Charge depletion and accumulation is represented by blue and red colors, respectively. (b) The partial density of states of O_2^- molecules adsorbed on $H_{atop\text{-}O}/\alpha$-$Al_2O_3(0001)$. The inset gives the isosurface of the spin density. (c) Calculated XAS and XMCD spectra of the oxygen K edge for O_2^- molecules associated with $H_{atop\text{-}O}/\alpha$-$Al_2O_3(0001)$.

O_2 in the $H_{atop\text{-}O} + O_2^-$ complex as shown in Fig. 3(b). In the unoccupied branch, the components of $m = \pm 1$ (where m is the magnetic quantum number) have different weights because of the joint effect of magnetization and spin-orbit coupling. The selection rules for dipole transitions ensure that left-circularly polarized light (LCPL) excites electrons from $1s$ core states ($m = 0$) to the branch of $m = 1$ of the unoccupied π^*_{2p} state, whereas right-circularly polarized light (RCPL) excites electrons to the branch of $m = -1$. The imbalance between $m = \pm 1$ components leads to different absorptions of LCPL and RCPL and hence produces an XMCD peak at the onset of the k edge of O_2^- as seen in Fig. 3(c). The XAS has more features in the higher energy region due to transitions to other orbitals.

We now consider ways to reduce the flux noise produced by H atoms embedded in α-$Al_2O_3(0001)$ or adsorbed on its surface. The binding energy of $H_{atop\text{-}O}$ is too large to remove these atoms by annealing. We propose using graphene as a protective coating due to its high structural stability and electron affinity to (1) reduce the $H_{atop\text{-}O}$-induced magnetization through charge transfer to the graphene; and (2) prevent H_2O, O_2, and other molecules from reaching the surface. Graphene has a small lattice mismatch (~1%) with α-$Al_2O_3(0001)$, and our calculations indicate that it binds strongly to $H_{atop\text{-}O}/\alpha$-$Al_2O_3(0001)$, with a binding energy of -0.65 eV/per unit cell. Al loses its excess charge to the adjacent C $2p_z$ orbitals of graphene due to the charge density difference shown in Fig. 4(a). As a result, the graphene bands shift downward [see Fig. 4(b)] and, importantly, the magnetic moment of $H_{atop\text{-}O}/\alpha$-$Al_2O_3(0001)$ is completely quenched [see leftmost bar at the bottom of Fig. 4(c)]. Figure 4(c) also shows that atomic hydrogen chemisorbed on top of graphene acquires a magnetic moment of 1 Bohr magneton [39]. To see if $H_{atop\text{-}O}$ can diffuse across graphene, we performed DFT calculations and found that the highest energy barrier for this diffusion is 5.1 eV [see Fig. 4(c)], implying that such diffusion is essentially blocked. Therefore, a graphene coating could effectively reduce flux noise by quenching the spin moment of H and by preventing the adsorption and diffusion of other gas molecules.

In summary our systematic DFT calculations demonstrate that H atoms embedded in (H_{inters}) or adsorbed on ($H_{atop\text{-}O}$) α-$Al_2O_3(0001)$ have sizable magnetic moments that can produce $1/f$ flux noise, owing to their small MAEs (a few millikelvin) and moderate exchange interactions. In addition, $H_{atop\text{-}O}$ may also strongly attract gas molecules from the environment, resulting in additional sources of flux noise. We propose coating Al SQUIDs with a layer of graphene that would not only protect the surface from other gas molecules, but also eliminate the magnetism produced by adsorbed H

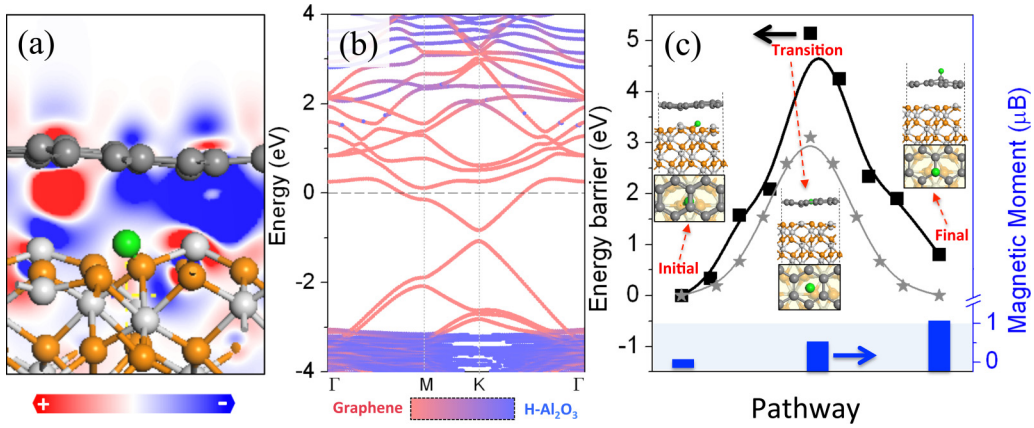

FIG. 4. (a) Atomic geometry and charge redistribution of graphene/$H_{atop\text{-}O}/\alpha$-$Al_2O_3(0001)$. Charge depletion and accumulation are represented by blue and red, respectively. (b) Electronic band structure of graphene/$H_{atop\text{-}O}/\alpha$-$Al_2O_3(0001)$ in a folded two-dimensional Brillouin zone for the 2×2 supercell. The color bar indicates their relative weights in graphene and $H_{atop\text{-}O}/\alpha$-$Al_2O_3(0001)$. Horizontal black line represents the Fermi level. (c) The relative total energy as the H atom diffuses across graphene over α-$Al_2O_3(0001)$, accompanied by the corresponding results for H diffusing through a freestanding graphene (gray line). Insets are the top and side views of atomic configurations for H being below and above graphene. Bars at the bottom show the calculated magnetic moments of graphene/$H_{atop\text{-}O}/\alpha$-$Al_2O_3(0001)$ in different configurations.

atoms. Our studies provide insights and strategies for reducing sources of magnetic noise in superconducting circuits.

Work at UCI was supported by DOE-BES (H.W. and R.Q.W., Grant No. DE-FG02-05ER46237). Work at Fudan (Z.W.) was supported by the National Science Foundation of China under Grant No. 11474056 and National Basic Research Program of China under Grant No. 2015CB921400. C.C.Y. was supported in part by a gift from Google (Google Gift No. 2502) and a grant from the UC Office of the President Multicampus Research Programs and Initiatives (MRP-17-454755). Computer simulations were performed at the U.S. Department of Energy Supercomputer Facility (NERSC).

Z.W. and H.W. contributed equally to this work.

[1] P. K. Day, H. G. LeDuc, B. A. Mazin, A. Vayonakis, and J. Zmuidzinas, Nature (London) **425**, 817 (2003).
[2] A. Fleischmann, C. Enss, and G. M. Seidel, *Cryogenic Particle Detection* (Springer-Verlag, Berlin, 2005).
[3] C. A. Regal, J. D. Teufel, and K. W. Lehnert, Nat. Phys. **4**, 555 (2008).
[4] X. Mi, J. V. Cady, D. M. Zajac, P. W. Deelman, and J. R. Petta, Science **355**, 156 (2017).
[5] A. Stockklauser, P. Scarlino, J. V. Koski, S. Gasparinetti, C. K. Andersen, C. Reichl, W. Wegscheider, T. Ihn, K. Ensslin, and A. Wallraff, Phys. Rev. X **7**, 011030 (2017).
[6] M. Hatridge, R. Vijay, D. H. Slichter, J. Clarke, and I. Siddiqi, Phys. Rev. B **83**, 134501 (2011).
[7] P. Kumar, S. Sendelbach, M. A. Beck, J. W. Freeland, Z. Wang, H. Wang, C. C. Yu, R. Q. Wu, D. P. Pappas, and R. McDermott, Phys. Rev. Appl. **6**, 041001 (2016).
[8] S. E. de Graaf, A. A. Adamyan, T. Lindström, D. Erts, S. E. Kubatkin, A. Y. Tzalenchuk, and A. V. Danilov, Phys. Rev. Lett. **118**, 057703 (2017).
[9] S. E. de Graaf, L. Faoro, J. Burnett, A. Adamyan, A. Y. Tzalenchuk, S. Kubatkin, T. Lindström, and A. Danilov, Nat. Commun. **9**, 1143 (2018).
[10] B. G. Levi, Phys. Today **62**, 14 (2009).
[11] H. Bluhm, N. C. Koshnick, J. A. Bert, M. E. Huber, and K. A. Moler, Phys. Rev. Lett. **102**, 136802 (2009).
[12] R. H. Koch, D. P. DiVincenzo, and J. Clarke, Phys. Rev. Lett. **98**, 267003 (2007).
[13] S. Sendelbach, D. Hover, A. Kittel, M. Mück, J. M. Martinis, and R. McDermott, Phys. Rev. Lett. **100**, 227006 (2008).
[14] H. Bluhm, J. A. Bert, N. C. Koshnick, M. E. Huber, and K. A. Moler, Phys. Rev. Lett. **103**, 026805 (2009).
[15] S. M. Anton, J. S. Birenbaum, S. R. O'Kelley, V. Bolkhovsky, D. A. Braje, G. Fitch, M. Neeley, G. C. Hilton, H.-M. Cho, K. D. Irwin, F. C. Wellstood, W. D. Oliver, A. Shnirman, and J. Clarke, Phys. Rev. Lett. **110**, 147002 (2013).
[16] S. Sendelbach, D. Hover, M. Mück, and R. McDermott, Phys. Rev. Lett. **103**, 117001 (2009).
[17] J. Wu and C. C. Yu, Phys. Rev. Lett. **108**, 247001 (2012).
[18] D. Lee, J. L. DuBois, and V. Lordi, Phys. Rev. Lett. **112**, 017001 (2014).
[19] H. Wang, C. Shi, J. Hu, S. Han, C. C. Yu, and R. Q. Wu, Phys. Rev. Lett. **115**, 077002 (2015).
[20] C. M. Quintana, Y. Chen, D. Sank, A. G. Petukhov, T. C. White, D. Kafri, B. Chiaro, A. Megrant, R. Barends, B. Campbell, Z. Chen, A. Dunsworth, A. G. Fowler, R. Graff, E. Jeffrey, J. Kelly, E. Lucero, J. Y. Mutus, M. Neeley, C. Neill, P. J. J. O'Malley, P. Roushan, A. Shabani, V. N. Smelyanskiy, A. Vainsencher, J. Wenner, H. Neven, and J. M. Martinis, Phys. Rev. Lett. **118**, 057702 (2017).
[21] G. Kresse and J. Furthmüller, Phys. Rev. B **54**, 11169 (1996).
[22] G. Kresse and J. Hafner, Phys. Rev. B **49**, 14251 (1994).
[23] J. P. Perdew, K. Burke, and M. Ernzerhof, Phys. Rev. Lett. **77**, 3865 (1996).
[24] H. J. Monkhorst and J. D. Pack, Phys. Rev. B **13**, 5188 (1976).
[25] S. Grimme, J. Antony, S. Ehrlich, and H. Krieg, J. Chem. Phys. **132**, 154104 (2010).
[26] H. Wang, S. Li, H. He, A. Yu, F. Toledo, Z. Han, W. Ho, and R. Q. Wu, J. Phys. Chem. Lett. **6**, 3453 (2015).
[27] S. W. Li, A. Yu, F. Toledo, Z. M. Han, H. Wang, H. Y. He, R. Q. Wu, and W. Ho, Phys. Rev. Lett. **111**, 146102 (2013).
[28] R. Q. Wu and A. J. Freeman, J. Magn. Magn. Mater. **200**, 498 (1999).
[29] E. Wimmer, H. Krakauer, M. Weinert, and A. J. Freeman, Phys. Rev. B **24**, 864 (1981).
[30] X. D. Wang, R. Q. Wu, D. S. Wang, and A. J. Freeman, Phys. Rev. B **54**, 61 (1996).
[31] J. Hu and R. Q. Wu, Phys. Rev. Lett. **110**, 097202 (2013).
[32] H. Wang, Y. N. Zhang, R. Q. Wu, L. Z. Sun, D. S. Xu, and Z. D. Zhang, Sci. Rep. **3**, 3521 (2013).
[33] See Supplemental Material at http://link.aps.org/supplemental/10.1103/PhysRevB.98.020403 for the AIMD simulations.
[34] K. C. Hass, W. F. Schneider, A. Curioni, and W. Andreoni, Science **282**, 265 (1998).
[35] L. Gordon, H. Abu-Farsakh, A. Janotti, and C. G. Van de Walle, Sci. Rep. **4**, 7590 (2014).
[36] Y.-H. Lu and H.-T. Chen, Phys. Chem. Chem. Phys. **17**, 6834 (2015).
[37] A. B. Belonoshko, A. Rosengren, Q. Dong, G. Hultquist, and C. Leygraf, Phys. Rev. B **69**, 024302 (2004).
[38] G. Henkelman, B. P. Uberuaga, and H. Jónsson, J. Chem. Phys. **113**, 9901 (2000).
[39] H. González-Herrero, J. M. Gómez-Rodríguez, P. Mallet, M. Moaied, J. J. Palacios, C. Salgado, M. M. Ugeda, J.-Y. Veuillen, F. Yndurain, and I. Brihuega, Science **352**, 437 (2016).